Hindawi Publishing Corporation
Journal of Nanomaterials
Volume 2014, Article ID 492832, 7 pages
http://dx.doi.org/10.1155/2014/492832

Research Article

Microstructure and Superparamagnetic Properties of Mg-Ni-Cd Ferrites Nanoparticles

M. M. Eltabey,[1,2] A. M. Massoud,[3,4] and Cosmin Radu[5]

[1] *Basic Engineering Science Department, Faculty of Engineering, Menoufiya University, Menoufiya, Egypt*
[2] *Science Department, Faculty of Medicine, Jazan University, Jazan, Saudi Arabia*
[3] *Physics Department, Faculty of Science, Ain Shams University, Abbassia, Cairo 11566, Egypt*
[4] *Physics Department, Faculty of Science, Jazan University, Jazan, Saudi Arabia*
[5] *Lake Shore Cryotronics, Inc., Westerville, OH, USA*

Correspondence should be addressed to M. M. Eltabey; mohamed.eltabey@yahoo.com

Received 10 February 2014; Revised 22 April 2014; Accepted 5 May 2014; Published 26 May 2014

Academic Editor: Ping Xiao

Magnesium substituted nickel cadmium ferrite nanoparticles $Mg_xNi_{0.6-x}Cd_{0.4}Fe_2O_4$ (from $x = 0$ to 0.6 with step 0.1) have been synthesized by the chemical coprecipitation route. X-ray diffraction (XRD) and infrared spectroscopy (FTIR) revealed that the obtained powders have a single phase of cubic spinel structure. The crystallite sizes calculated from XRD data have been confirmed using transmission electron microscopy (TEM) showing that the powders are consisting of nanosized grains with an average size range 5–1.5 nm. Magnetic hysteresis loops were traced at 6.5 K as well as at room temperature using VSM. It was found that, due to the Mg^{2+}-ions substitution, the values of saturation magnetization M_s for the investigated samples were decreased, whereas the coercive field H_c increased. Both zero field cooling (ZFC) and field cooling (FC) curves are measured in the temperature range (6.5–350 K) and the values of blocking temperature T_B were determined. No considerable variation in the values of T_B was observed with increasing Mg-content, whereas the values of the effective anisotropy constant K_{eff} were increased.

1. Introduction

Ferrites have drawn the attention for decades for their wide range of applications. Technological and industrial applications of ferrites depend mostly on their distinguishable magnetic and electric properties. Microwave devices, ferrofluids, and storage media of computers are the most important applications that make use of ferrites properties [1–3]. Structural and magnetic properties of ferrites are varying with the preparation methods as well as with the kind of substituting ions. Nanoferrites show special magnetic and electric properties which are quite different from the bulk ferrites [4]. Nickel substituted ferrites are considered to be the most versatile and found wide spread application in the electronics and microwave devices due to their high electrical resistivity, low eddy current, and dielectric loss [5]. Nickel cadmium (Ni-Cd) ferrite has many microwave applications for its high value of coercivity, remanence, and saturation magnetization [3]. $Cd_xNi_{1-x}Fe_2O_4$ was investigated by Shelar et al. [6] and the saturation magnetization showed an increase with the Cd-content. Magnesium ferrite is a soft magnetic material that is utilized in transformer cores and catalysts [7, 8]. In addition, Liu reported that magnesium containing ferrites is preferred to obtain high resistivity and avoid the tendency of discontinuous grain growth to have dense ferrite [9]. The influence of the nonmagnetic Mg^{2+}-ions as a substitutant for magnetic Ni^{2+}-ions on the different ferrite systems has been investigated by studying structural and magnetic properties of these ferrite samples [10, 11]. A significant increase in the initial permeability was determined at Ni-content of 0.3 (Mg-content = 0.2) in $Ni_xMg_{0.5-x}Cu_{0.1}Zn_{0.4}Fe_2O_4$ ferrite system [10]. Therefore, it is expected that the structural and magnetic properties of Ni-Cd ferrites could show a remarkable variation by Mg^{2+} substitution. In the current work, Mg^{2+}-ions are substituted in

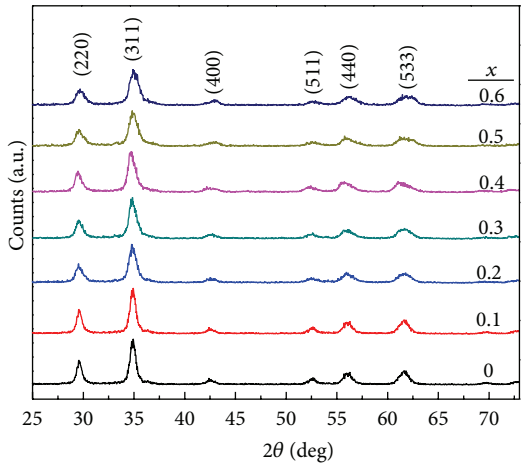

FIGURE 1: X-ray diffraction pattern of the system $Mg_xNi_{0.6-x}Cd_{0.4}Fe_2O_4$.

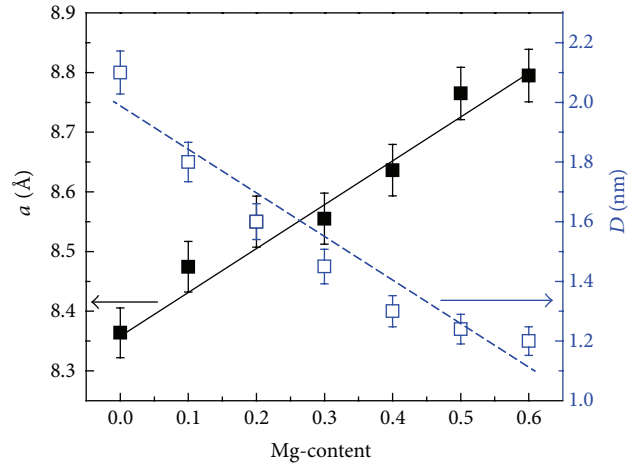

FIGURE 2: Changeof the lattice parameter a (Å) and the crystallite size D (nm) with Mg-content of the system $Mg_xNi_{0.6-x}Cd_{0.4}Fe_2O_4$.

the nanoferrite system $Ni_{0.6}Cd_{0.4}Fe_2O_4$ which was reported to give reasonable high magnetic values [6]. Nanoparticle samples of the ferrite system $Mg_xNi_{0.6-x}Cd_{0.4}Fe_2O_4$ (x = 0–0.6 with step 0.2) were synthesized and studied in a wide range of temperatures.

2. Materials and Methods

Magnesium nickel cadmium nanoferrites ($Mg_xNi_{0.6-x}Cd_{0.4}Fe_2O_4$, x = 0,0.1,0.2,0.3,0.4,0.5,0.6) were synthesized via the chemical coprecipitation method using $NiSO_4{\cdot}6H_2O$, $MgSO_4{\cdot}7H_2O$, $CdCl_2{\cdot}H_2O$, $FeCl_3$, and NaOH. Salts were mixed in the required stoichiometric ratios in deionized water. Sodium hydroxide (NaOH) solution was then added dropwise, while stirring, until the measured pH value was 12. The mixture was continually stirred at 700 rpm for two hours while being heated at 353 K. A dark color was observed due to the formation of the ferrite particles. Particles were allowed to settle and the mixture was washed several times until the measured pH value was about 7. The powder sample was then allowed to dry at room temperature. X-ray diffraction (XRD) patterns were performed using the diffractometer of type Philips and they were identified by CuK_α radiation (λ = 1.5418 Å). The (311) reflection line in XRD pattern was used to calculate the average crystallite size D using the Debye-Scherrer equation, $D = (0.9\lambda)/(\beta\cos\theta)$ [12], where β is the full width at half-maximum FWHM of the diffraction line and θ is the corresponding diffraction angle. The grain micrograph was obtained by low vacuum TEM JEOL (JEM-1400 TEM). FTIR spectra were carried out (using Perkin Elmer spectrophotometer) in the wavenumbers range 150–650 cm^{-1}. Hysteresis loops were obtained at low temperature (6.5 K) as well as at room temperature using a Model 7410 Lake Shore Cryotronics Vibrating Sample Magnetometer (VSM). The results are normalized and displayed as saturation magnetization M_s (emu/g) versus field H (Oe).

3. Results and Discussion

3.1. X-Ray and TEM Analysis. XRD patterns in Figure 1 indicate that all samples are formed in single phase of cubic spinel structure. The values of d-spacing are calculated according to Bragg's law and hence the average lattice parameter a (Å) is determined. Variation of lattice parameter with the concentration of Mg^{2+}-ions is plotted in Figure 2. It is clear that as the Mg-concentration increases the lattice parameter increases. Such a behavior was previously observed in Mg-substituted Ni-Cu-Zn ferrites [13]. The increase in lattice parameter could be explained on the basis of the ionic radii due to the replacement of ions with smaller ionic radius of Ni^{2+} (0.69 Å) by the larger ones of Mg^{2+} (0.72 Å). The composition dependence of crystallite size D is shown in Figure 2. It is obvious that D decreases slightly with increasing the Mg-content. The decrease of crystallite size due to Mg-substitution in Mg-Cd-Zn ferrites was reported in a previous work [14]. Such a behavior could be explained in the light of crystal growth process in a solution. It was reported that the crystal growth in a solution depends on various factors; the most important two are the following:

(i) the molecular concentration of the material approaching the surface of the tiny crystal during the growth process,

(ii) the site preferences of the cations in the ferrite system.

For the first factor (i), the local temperature is normally higher than the solution temperature due to the liberation of latent heat at the surface. The surface temperature affects the molecular concentration at the surface of the crystal and, hence, the crystal growth rate [15]. For the second one (ii), the grain growth is obstructed when the cationic preferences are not fully satisfied [16]. In view of these factors and the obtained behavior of D, one can conclude that as the Mg-content increases more heat may be liberated. This leads to a decrease in the molecular concentration at the crystal surface and hence obstructing the grain growth.

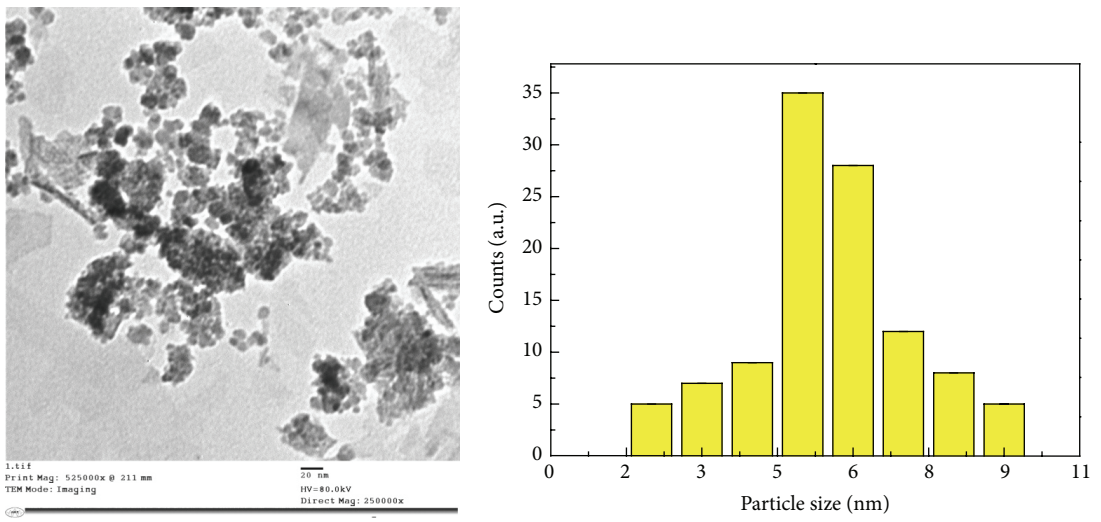

(a) (b)

FIGURE 3: TEM micrograph for sample with $x = 0$ (a) and its particle size distribution (b).

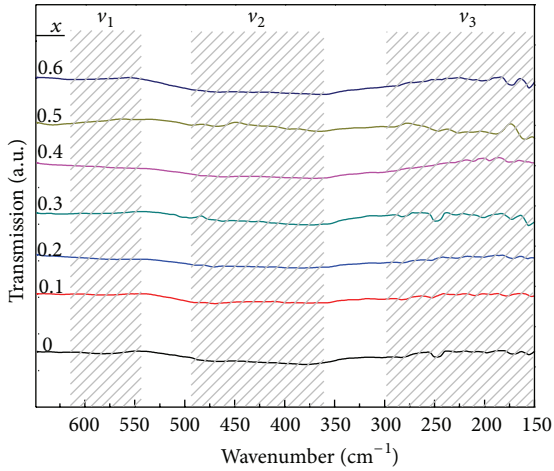

FIGURE 4: FTIR spectra of the system $Mg_xNi_{0.6-x}Cd_{0.4}Fe_2O_4$.

Furthermore, according to the assumed cation distribution (Section 3.3), the tendency of both Mg^{2+}- and Ni^{2+}-ions to occupy B-sites leads to the migration of some Ni^{2+}-ions from B- to A-sites although its high preference for B-sites occupation. This shows that the presence of Mg^{2+}- and Ni^{2+}-ions together makes the cationic preference not satisfied fully leading to the decrease of the rate of crystal growth.

Transmission electron micrograph TEM was performed for the unsubstituted sample with $x = 0$, as an example, and it is represented in Figure 3(a). The micrograph reveals that the obtained particles are spherical in shape and have a dominant value of diameter of about 5 nm. The particle size distribution that is obtained from TEM micrograph is represented by a histogram as shown in Figure 3(b).

3.2. FTIR Spectra Analysis. The study of far-infrared spectrum is an important tool to get information about the position of ions in the crystal through the vibrational modes [17]. According to the group theory, the normal and inverse cubic spinel should have individual bands for the tetrahedral and octahedral complexes and another one for lattice vibrations [17, 18]. Figure 4 shows the FTIR spectra for the investigated samples in the wave number ranging from 150 to 650 cm^{-1}. The given absorption bands from the spectrophotometer showed that there exist three fundamental bands $\{\nu_1, \nu_2, \nu_3\}$ confirming that the present system is formed in a cubic inverse spinel structure as was discussed in Section 3.1 [19]. It has been reported that the first two IR fundamental bands are due to tetrahedral and octahedral complexes, while the third one is due to the lattice vibrations [17]. IR spectra show no sharp peaks due to the extremely small particle size and therefore the limitation of the crystallinity in the current investigated samples. The high frequency band ν_1 (616–548 cm^{-1}) is attributed to the vibration of iron ions in the tetrahedral positions. The second band ν_2 (363–494 cm^{-1}) is associated with the iron ions with divalent octahedral metal ions and oxygen complexes. Finally, the third vibrational band (less than 300 cm^{-1}) is attributed to the lattice vibrational frequency [20]. Figure 5(a) shows the variation of ν_1 and the values of A-sites radii r_A with the increase of the Mg-content. An increasing trend in values of ν_1 is noticed. This behavior could be attributed to the decrease in r_A which was calculated according to the assumed cation distribution taking into consideration that the values of the ionic radii are depending on the coordination number [21]. The cation distribution will be discussed in detail later. The decrease of r_A with Mg-content could be explained in the light of that distribution given in (1). Whereas the Mg-concentration increases in B-sites, the amount of Fe^{3+}-ions ($r_{Fe^{3+}} = 0.49$ Å) increases in A-sites on the expense of Ni^{2+}-ions ($r_{Ni^{2+}} = 0.55$ Å). That decrease of r_A leads to making the bond shorter/stronger, leading to an increase in the values of ν_1. On the other hand, Figure 5(b) shows the variation

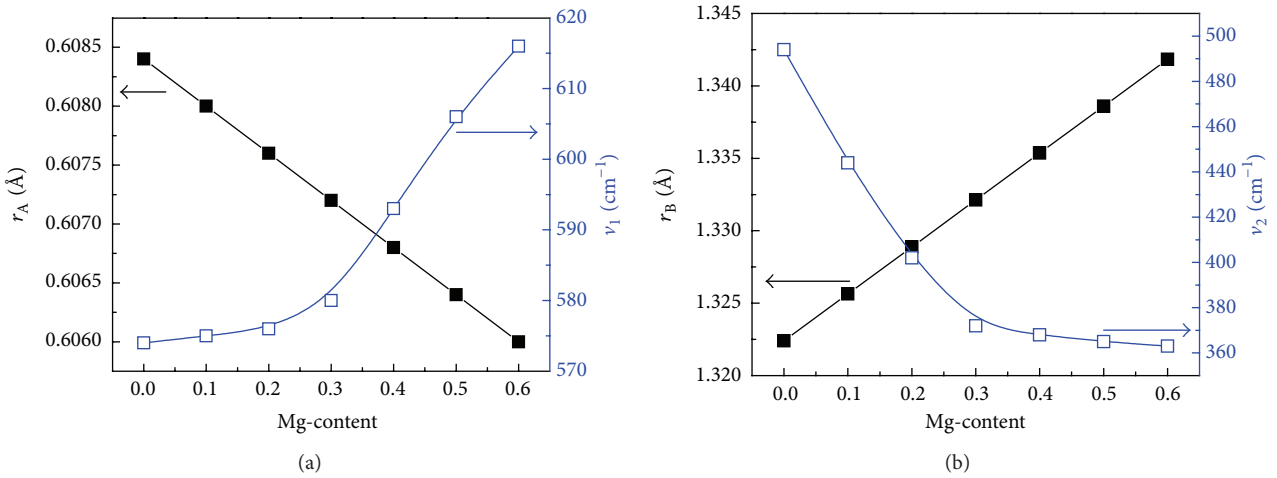

FIGURE 5: (a) Composition dependence of A-sites radii with the variation of the tetrahedral and (b) composition dependence of B-sites radii with the variation of the octahedral band in the system $Mg_xNi_{0.6-x}Cd_{0.4}Fe_2O_4$.

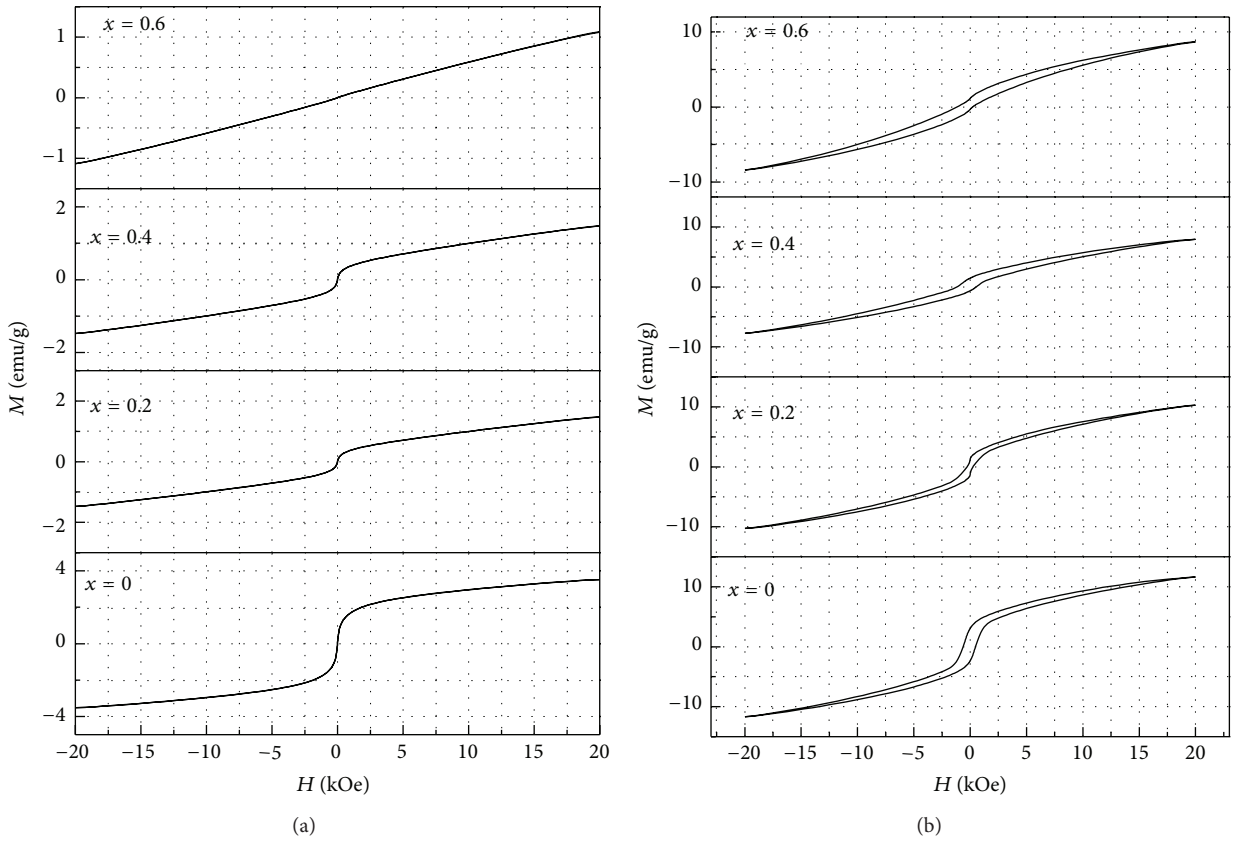

FIGURE 6: Hysteresis loops of the system $Mg_xNi_{0.6-x}Cd_{0.4}Fe_2O_4$ (x = 0, 0.2, 0.4, and 0.6) at (a) room temperature and (b) 6.5 k.

of ν_2 and the values of B-sites radii r_B with Mg-content. It is obvious that ν_2 dramatically decreases whereas r_B linearly increases with increasing the Mg-content. That decrease of ν_2 could be understood and explained by the increase of r_B. According to the assumed cation distribution, as the Mg-concentration increases in B-site ($r_{Mg^{2+}}$ = 0.72 Å), both the amount of Fe^{3+}-ions ($r_{Fe^{3+}}$ = 0.65 Å) and amount of Ni^{2+}-ions ($r_{Ni^{2+}}$ = 0.69 Å) are decreasing. The decrease of r_A leads to making the bond longer/weaker, leading to a decrease in the values of ν_2.

3.3. Magnetic Properties. Hysteresis loops at room temperature (300 K) and at low temperature (6.5 K) for samples with x = 0, 0.2, 0.4, and 0.6 are shown in Figures 6(a) and 6(b).

It is clear from Figure 6(a) that the loops for the samples that are measured at room temperature are closed ones, showing almost no coercivity, which is considered to be a typical superparamagnetic behavior. There is no full saturation behavior observed even near the high values of magnetic field for all the investigated samples which could be attributed to the canted surface spins in nanoparticles [22]. The values of the slopes of the M-H curves increase as the Mg-content increases. This behavior could be referred to the decreasing of particle size with the Mg-content leading to an increase in the area to volume ratio. On the other hand, Figure 6(b) in which the loops are measured at 6.5 K shows open hysteresis loops indicating the presence of an ordered magnetic structure. Variations of the values of saturation magnetization M_s (emu/g) which are measured at 300 and 6.5 K with Mg-concentration are represented in Figure 7. It is clear that at 6.5 K the values of M_s are higher than those measured at 300 K with an average percentage of 77.4%. This behavior is mainly due to the thermal disorder of magnetic moments. It is obvious that, at both temperatures, as Mg-content increases, the values of M_s linearly decrease. This trend could be explained in the light of the following proposed cation distribution:

$$\begin{aligned}&\left(\mathrm{Cd}^{2+}_{0.4}\ \mathrm{Ni}^{2+}_{(0.04-0.06x)}\ \mathrm{Fe}^{3+}_{(0.56+0.06x)}\right)_{\mathrm{A}}\\&\left[\mathrm{Mg}^{2+}_{x}\ \mathrm{Ni}^{2+}_{(0.56-0.94x)}\ \mathrm{Fe}^{3+}_{(1.44-0.06x)}\right]_{\mathrm{B}}.\end{aligned}\tag{1}$$

That distribution is assumed according to the following bases.

(1) Cadmium ions prefer to occupy the tetrahedral sites (A-sites) [5, 23].

(2) Magnesium preferential sites are the octahedral ones (B-sites) [11, 24].

(3) It was reported that Ni^{2+}-ions are distributed between the tetrahedral and octahedral sites such that the majority of these ions (about 94%) are located into the B-sites [11, 24].

According to the above cation distribution, the net magnetization (M) could be calculated as follows: $M = M_{\mathrm{B}} - M_{\mathrm{A}}$, where M_{B} and M_{A} are the magnetic moments of the octahedral and tetrahedral sites, respectively. Using the values of the magnetic moments of Fe^{3+}, Ni^{2+}, Mg^{2+}, and Cd^{2+} as 5, 2, 0, and 0 μ_{B}, respectively, the total magnetic moment could be written as

$$M = 5.44 - 2.36x. \tag{2}$$

Equation (2) represents a linear relationship between the Mg^{2+}-ions concentration (x) and the magnetization value (M) which is in agreement with the obtained experimental behavior (cf. Figure 7). This agreement supports the validity of the assumed cation distribution.

The coercivity H_c is automatically determined for the measured loops at 6.5 K and it is plotted as an inset in Figure 7. It is obvious that, in average, H_c is increasing with the increase of the Mg-concentration with an acceptable anomaly

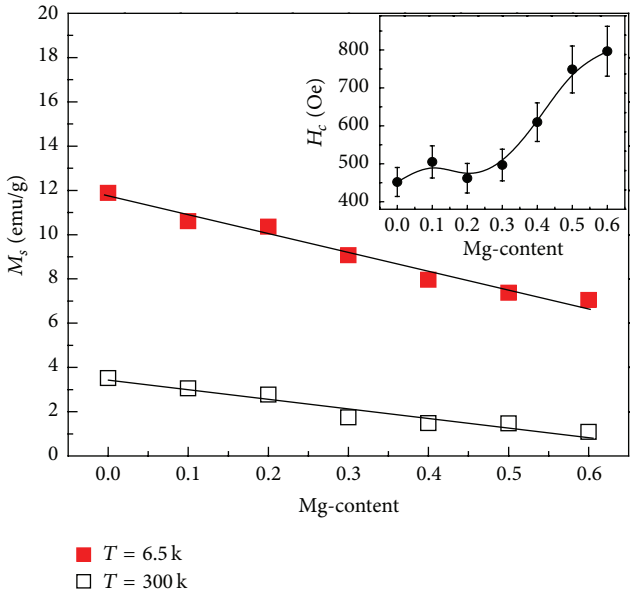

Figure 7: Composition dependence of saturation magnetization at low and room temperature of the system $Mg_xNi_{0.6-x}Cd_{0.4}Fe_2O_4$. Inset shows the composition dependence of the coercive field at low temperature.

at $x = 0.2$. This behavior could be explained according to Brown's relation [25]:

$$H_c \geq \frac{(2K_{\mathrm{eff}})}{(\mu_o M_s)}, \tag{3}$$

where K_{eff} is the effective anisotropy constant, μ_o is the magnetic permeability, and M_s is the saturation magnetization. The increase in the values of H_c with Mg-content could be attributed to the decrease of M_s as the magnesium concentration increases, in addition to the increase of the values of the effective anisotropy constant K_{eff} with the increasing of Mg-content as will be discussed hereafter.

The temperature dependence of ZFC- and FC-magnetization at 1 kOe for the current investigated samples is shown in Figure 8. The peaks in ZFC-curves determine the values of the blocking temperature T_B. This phenomenon is called superparamagnetism and it is often observed in the nanoparticles in which each nanoscaled particle is considered to be a single magnetic domain [26]. The thermal energy at $T > T_B$ is sufficient to induce fluctuations in the magnetization. The observed magnetization would depend on the measurement time t_m relative to the relaxation time τ of thermal fluctuations. This relaxation time τ for a single particle is given by [26]

$$\tau = \tau_o \exp\left(\frac{K_{\mathrm{eff}}V}{k_B T}\right), \tag{4}$$

where a characteristic time τ_o is typically 10^{-9} s, and k_BT, K_{eff}, and V are, respectively, the thermal energy, the effective

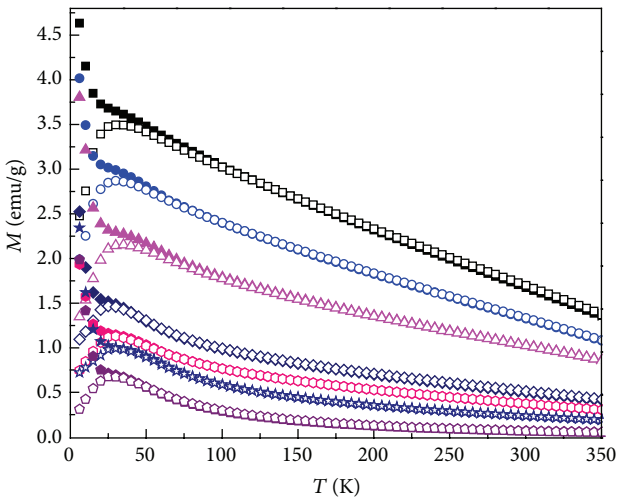

FIGURE 8: ZFC- and FC-magnetization curves of the system $Mg_xNi_{0.6-x}Cd_{0.4}Fe_2O_4$. The blocking temperature values are listed in the legend box.

magnetic anisotropy constant, and the particle volume. The blocking temperature is then

$$T_B = \frac{K_{\text{eff}}V}{[k_B \ln(t_m/\tau_o)]}, \quad (5)$$

with the measuring time $t_m = \tau$.

By assuming $t_m/\tau_o = 10^{11}$ in a typical magnetization measurement, one arrives at the commonly cited equation:

$$T_B = \frac{K_{\text{eff}}V}{25k_B}. \quad (6)$$

The values of blocking temperature T_B are determined from the peak of ZFC-curve for each sample and they are listed inside Figure 8. It is clear that the blocking temperature shows no considerable variation with the Mg-content. This could be explained according to (6) as follows.

As the Mg-content increases, the particle volume ($V = (\pi/6)D^3$) decreases (cf. Figure 2) leading to decreasing the values of T_B. On the other hand, it was reported that the values of the effective anisotropy constant for Mg-Zn and Ni-Zn ferrites are 10^5 and 1.7×10^4 J/m^3, respectively [27, 28]. This means that the presence of magnesium in such ferrites enhances the values of K_{eff}. Thus, the increase of Mg-content leads to an increase in T_B. In other words, the almost constancy of T_B could be attributed to the competition between the increase of anisotropy constant and the decrease

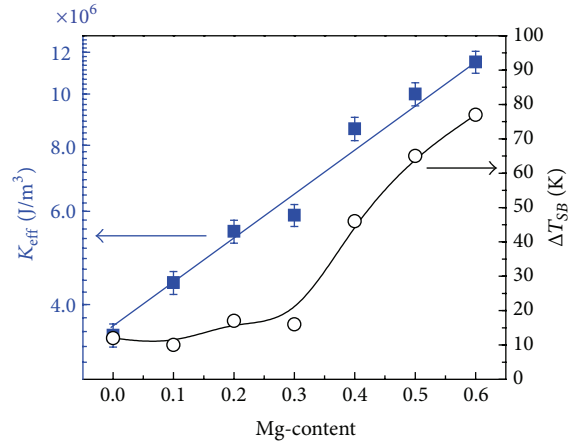

FIGURE 9: Composition dependence of the anisotropy constant and the splitting range of the system $Mg_xNi_{0.6-x}Cd_{0.4}Fe_2O_4$.

in the particle size with increasing Mg-content. The increase of the calculated values of the anisotropy constant with Mg-content for the present samples is illustrated in Figure 9.

Figure 8 shows also that, for all investigated samples, there is a coincidence between the values of ZFC- and FC-magnetization down to a certain temperature (referred to as T_S) at which the splitting between the two curves begins to take place. According to (6), each particle size (V) meets a certain value of blocking temperature (T_B). This means that when all the particles in the sample have the same size (maximum homogeneity) there will be a coincidence between the values of T_B and T_S with a sharp peak in ZFC-curve. The above discussion reveals that, as the homogeneity is destroyed, the difference between T_S and T_B ($\Delta T_{SB} = T_S - T_B$) will increase. The composition dependence of ΔT_{SB} for the current investigated samples is illustrated in Figure 9. It is clear that as Mg-content increases, ΔT_{SB} increases, indicating that magnesium destroys homogeneity.

4. Conclusion

Taken together, we provide the following conclusions.

(i) The chemical coprecipitation technique has been used for the synthesis of a single spinel cubic phase of $Mg_xNi_{0.6-x}Cd_{0.4}Fe_2O_4$ ferrite nanoparticles with Mg-concentration up to 0.6.

(ii) The values of lattice parameter were increased due to the Mg-substitution whereas the calculated crystallite size decreased slightly.

(iii) Mg-substitution in Ni-Cd ferrites leads to a decrease in the values of the saturation magnetization and an increase in the values of coercive field.

(iv) No considerable variation was observed in the values of the blocking temperature with increasing Mg-content, whereas the values of the effective anisotropy constant were increased.

Conflict of Interests

The authors declare that there is no conflict of interests regarding the publication of this paper.

Acknowledgment

The authors would like to acknowledge Lake Shore Cryotronics, Inc., Westerville, OH, USA, for supporting the publishing of this paper.

References

[1] A. S. Waingankar, S. G. Kulkarni, and M. S. sagare, "Humidity sensing using soft ferrites," *Journal de Physique IV*, vol. 7, no. 1, pp. 155–156, 1997.

[2] O. H. kwon, Y. Fukushima, M. Sugimoto, and N. Hirotsuka, "Thermocouple junctioned with ferrites," *Journal de Physique IV*, vol. 7, no. 1, pp. 165–166, 1997.

[3] M. B. Shelar, P. A. Jadhav, S. S. Chougule, M. M. Mallapur, and B. K. Chougule, "Structural and electrical properties of nickel cadmium ferrites prepared through self-propagating auto combustion method," *Journal of Alloys and Compounds*, vol. 476, no. 1-2, pp. 760–764, 2009.

[4] R. Sridhar, D. Ravinder, and K. V. Kumar, "Synthesis and characterization of copper substituted nickel nano-ferrites by citrate-gel technique," *Advances in Materials Physics and Chemisty*, vol. 2, no. 3, pp. 192–199, 2012.

[5] K. S. Lohar, S. M. Patange, M. L. Mane, and E. Sagar Shirsath, "Cation distribution investigation and characterizations of $Ni_{1-x}Cd_xFe_2O_4$ nanoparticles synthesized by citrate gel process," *Journal of Molecular Structure*, vol. 1032, pp. 105–110, 2013.

[6] M. B. Shelar, P. A. Jadhav, D. R. Patil, B. K. Chougule, and V. Puri, "Chemical synthesis and studies on structural and magnetic properties of fine grained nickel cadmium ferrites," *Journal of Magnetism and Magnetic Materials*, vol. 322, no. 21, pp. 3355–3358, 2010.

[7] S. Burianova, J. Poltierova-Vejpravova, P. Holec, and J. Plocek, "Magnetocaloric phenomena in Mg-ferrite nanoparticles," *Journal of Physics: Conference Series*, vol. 200, section 7, Article ID 072015, 2010.

[8] Y. Ichiyanagi, M. Kubota, S. Moritake, Y. Kanazawa, T. Yamada, and T. Uehashi, "Magnetic properties of Mg-ferrite nanoparticles," *Journal of Magnetism and Magnetic Materials*, vol. 310, no. 2, pp. 2378–2380, 2007.

[9] D.-M. Liu, "Sintering of $(Ca_{1-x}, Mg_x)Zr_4(PO_4)_6$ ceramics," *Journal of Materials Science*, vol. 29, no. 6, pp. 1507–1513, 1994.

[10] S. G. Bachhav, R. S. Patil, P. B. Ahirrao, A. M. Patil, and D. R. Patil, "Microstructure and magnetic studies of Mg-Ni-Zn-Cu ferrites," *Materials Chemistry and Physics*, vol. 129, no. 3, pp. 1104–1109, 2011.

[11] M. U. Rana, M. U. Islam, and T. Abbas, "X-Ray diffraction and site preference analysis of Ni-Substituted $MgFe_2O_4$ ferrites," *Pakistan Journal of Applied Sciences*, vol. 2, no. 12, pp. 1110–1114, 2002.

[12] B. D. Cullity, *Elements of X-Ray Diffraction*, Addison-Wesley, New York, NY, USA, 1956.

[13] C. Sujatha, K. V. Reddy, K. S. Babu, and K. H. Rao, "Structural and magnetic properties of $Ni_{0.5-x}Mg_xCu_{0.05}Zn_{0.45}Fe_2O_4$ ferrites for multilayer chip inductor applications," in *Proceedings of the International Conference on Nanoscience, Engineering and Technology (ICONSET '11)*, pp. 19–22, IEEE, Channai, India, November 2011.

[14] M. M. Eltabey, I. A. Ali, H. E. Hassan, and M. N. H. Comsan, "Effect of γ-rays irradiation on the structure and magnetic properties of Mg-Cu-Zn ferrites," *Journal of Materials Science*, vol. 46, no. 7, pp. 2294–2299, 2011.

[15] R. F. Strickland-Constable, *Kinetics and Mechanism of Crystallization*, Academic Press, New York, NY, USA.

[16] C. Rath, S. Anand, R. P. Das et al., "Dependence on cation distribution of particle size, lattice parameter, and magnetic properties in nanosize Mn-Zn ferrite," *Journal of Applied Physics*, vol. 91, no. 3, pp. 2211–2215, 2002.

[17] K. Mohan and Y. C. Venudhar, "Far-infrared spectra of lithium-cobalt mixed ferrites," *Journal of Materials Science Letters*, vol. 18, no. 1, pp. 13–16, 1999.

[18] D. Ravinder, "Far-infrared spectral studies of mixed lithium-zinc ferrites," *Materials Letters*, vol. 40, no. 5, pp. 205–208, 1999.

[19] A. A. Sattar, H. M. El-Sayed, K. M. El-Shokrofy, and M. M. El-Tabey, "Improvement of the magnetic properties of Mn-Ni-Zn ferrite by the non-magnetic Al^{3+}-Ion substitution," *Journal of Applied Sciences*, vol. 5, no. 1, pp. 162–168, 2005.

[20] M. A. Ahmed, E. Ateia, and S. I. El-Dek, "Spectroscopic analysis of ferrite doped with different rare earth elements," *Vibrational Spectroscopy*, vol. 30, no. 1, pp. 69–75, 2002.

[21] R. D. Shannon, Central Research and Development Department, Experimental Station, E. I. Du Pont de Nemours and Company, "Revised effective ionic radii and systematic studies of interatomic distances in halides and chalcogenides", Wilmington, Del, USA, Published in Acta Crystallographica. pp. 751-767, A32, 1976.

[22] B. Issa, I. M. Obaidat, B. A. Albiss, and Y. Haik, "Magnetic nanoparticles: surface effects and properties related to biomedicine applications," *International Journal of Molecular Sciences*, vol. 14, no. 11, pp. 21266–21305, 2013.

[23] A. B. Gadkari, T. J. Shinde, and P. N. Vasambekar, "Magnetic properties of rare earth ion (Sm^{3+}) added nanocrystalline Mg-Cd ferrites, prepared by oxalate co-precipitation method," *Journal of Magnetism and Magnetic Materials*, vol. 322, no. 24, pp. 3823–3827, 2010.

[24] E. Rezlescu, L. Sachelarie, P. D. Popa, and N. Rezlescu, "Effect of substitution of divalent ions on the electrical and magnetic properties of Ni-Zn-Me ferrites," *IEEE Transactions on Magnetics*, vol. 36, no. 6, pp. 3962–3967, 2000.

[25] C. J. Kriessman and S. E. Harrison, "Cation distributions in magnesium-nickel ferrites," *Journal of Applied Physics*, vol. 32, no. 3, pp. S392–S393, 1961.

[26] H. H. Hamdeh, W. M. Hikal, S. M. Taher et al., "Mössbauer evaluation of cobalt ferrite nanoparticles synthesized by forced hydrolysis," *Journal of Applied Physics*, vol. 97, no. 6, Article ID 064310, 2005.

[27] G. F. Barbosa, F. L. de Araujo Machado, A. R. Rodrigues, M. S. Silva, and A. Franco Jr., "Enhanced magnetic properties of Zn substituted Mg ferrite," *IEEE Transactions on Magnetics*, vol. 49, no. 8, pp. 4562–4564, 2013.

[28] S. Chikazumi, *Physics of Magnetism*, John Wiley & Sons, New York, NY, USA, 1964.